Non-equilibrium Energy Transfer and Phase Change during Intense Picosecond Laser-Metal Interactions

by

Long-Sheng Kuo

B.S., Mechanical Engineering
National Taiwan University, Taiwan(1991)

Submitted to the Department of Mechanical Engineering
in partial fulfillment of the requirements for the degree of

Master of Science in Mechanical Engineering

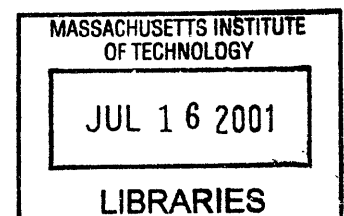at the

MASSACHUSETTS INSTITUTE OF TECHNOLOGY

June 2001

Author . . . .
Department of Mechanical Engineering
May 10, 2001

Certified by. . . . .
Taiqing Qiu
Associate Professor of Mechanical Engineering
Thesis Supervisor

Accepted by . . . .
Ain A. Sonin
Chairman, Department Committee on Graduate Students

Non-equilibrium Energy Transfer and Phase Change during Intense Picosecond Laser-Metal Interactions

by

Long-Sheng Kuo

Abstract

Laser interactions with metals involve absorption of photon energy by electrons, energy coupling between electrons and the lattice, and energy transport by diffusion of electrons and lattice vibrations. During picosecond laser irradiation of metal films, electrons and the lattice are not in thermal equilibrium. On the other hand, rapid laser heating produces a large degree of superheating and undercooling during melting and solidification. First, this work investigates experimentally non-equilibrium heating processes during intense picosecond laser heating of metal films. Results show excellent agreement with predictions of the two-step radiation heating model. Second, this work develops a general model to characterize both non-equilibrium energy deposition and phase change processes. The predictions show that the non-equilibrium heating processes significantly increase the laser melting threshold, enlarge the thermal-affected region, reduce the lattice temperature rise, prolong the phase change duration, and reduce the solidification speed. These results are important for materials processing using ultrashort pulsed lasers.

Acknowledgments

I thank my advisor, Professor Taiqing Qiu, for his advice, encouragement, and patience to me. His experimental expertise and experiences are what I learned from him most.

I also thank all of friends I met during this period. Although it is impossible to list them all, I'd especially like to thank Dr. Yu-Hsuan Su and Prof. Wentang Kuo. Without their friendships and helps, the graduate life at MIT would be much harder than it was.

Finally, and always, I thank my parents, who tolerate any of my carelessness and faults. I'd like to thank my sisters too, who take over my duties to take care of dad and mom.

Contents

List of Figures

List of Tables

Chapter 1

Introduction

1.1 Motivations

Lasers have unquestionably become an important part of the science and technology of since their invention. The high energy density and directionality achieved with lasers permits to observe and control processes on extraordinary spatial and temporal scales. Examples of their applications including material processing, laser diagnostics, optical communication, optical storage, holography, and medical imaging.

The ultrashort pulsed lasers provide fascinating potentials for material processing due to their unique features. For example, energy can be concentrated in a temporal interval as short as a few femtoseconds, which correspond to a few optical cycle in the visible range. Focusing a 50-fs laser pulse with energy of 0.1 mJ to a 100 μm^2 area yields an intensity of 2×10^{15} W/cm^2. Picosecond and femtosecond lasers have become increasingly important tools in manufacturing and bio-medical applications. Examples include nondestructive testing of microstructures by picosecond ultrasonics [1] and picosecond thermal waves [2],

synthesis of nanocrystalline materials [3], imaging individual molecules [4], and imaging living cells and tissues [5].

To describe the energy transfer during ultrashort laser irradiation, a two-step radiation heating model has been developed by Anisimov *et al.* [6] and Qiu and Tien [7]. This model has been compared qualitatively with experiments where the lattice-temperature rise is less than 5°C [8-15]. No work with quantitative comparions between experiments and model predictions has been reported. Morever, when the energy of laser pulses is high enough, phase change would occure. During such rapid heating, an extremely high temperature gradient would cause superheating and undercooling during phase change processes. The effects of the two-step model on this non-equilibrium melting and solidification have not been studied.

1.2 Objectives of This Work

The primary objectives in this research are (1) to experimentally determine the applicability of the two-step model and to establish regimes of non-equilibrium irradiation heating during intense picosecond laser pulse heating of metal films; and (2) to investigate theoretically non-equilibrium phase changes, e.g., superheating and undercooling, during picosecond laser pulse melting of metal films.

Chapter 2 presents the experimental investigations of 35-ps laser heating of gold films. To determine the validity of the two-step model, surface reflectivity is used in this research as an experimental parameter to indicate the electron temperature and lattice temperature during picosecond laser heating. Chapter 3 provides a non-equilibrium energy transfer and

non-equilibrium phase-change model to describe the intense ultrashort pulse laser-metal interactions. The results indicate that microscopic energy transfer and phase change are significant for picosecond laser processing of materials. Chapter 4 summarizes this work and proposes directions of further research.

Chapter 2

Experimental Investigations of Picosecond Laser Heating

2.1 Introduction

Due to the extremely intense energy transfer and short interaction time involved in picosecond and femtosecond applications, the applicability of the conventional Fourier heat conduction model is questionable. Anisimov *et al.* proposed a phenomenological model to describe microscopic energy transfer during laser-metal interactions [6]. The model describes absorption of photon energy by free electrons, energy coupling between electrons and the lattice, and energy transport through diffusion of electrons. This two-step radiation heating model was later derived rigorously from the Boltzmann transport equation by Qiu and Tien [7].

Non-equilibrium heating of electrons and lattice during femtosecond-metal interactions have been observed experimentally [8-15]. For example, rapid reflectivity changes were de-

12

tected following femtosecond laser heating pulses. The surface reflectivity reached steady state within a few picoseconds. The results suggest immediate heating of the electron system and the subsequent energy transfer between electrons and the lattice. In these experiments, the lattice-temperature rise is small (less than 5°C). Normalized results are compared with the theoretical predictions. Direct, quantitative comparisons, however, have not been performed. By assuming the reflectivity change is proportional to the change of electron temperature, Qiu and Tien found that the two-step radiation heating model can be used to accurately predict electron temperature and reflectivity changes during weak femtosecond laser heating [7,15]. The applicability of the two-step model during intense ultrashort light-metal interactions, however, has not been experimentally tested.

For picosecond laser applications, the significance of non-equilibrium electron-lattice heating has not been well understood. Eesley observed strong non-equilibrium electronic heating during 8-ps laser pulse heating in copper [9]. For relatively long and weak laser pulses (160 ps), Elsayed-Ali and Herman found that the effect of non-equilibrium radiation heating is small [16]. On the other hand, Rosenfeld and Campbell found that non-equilibrium electronic heating is significant even for 130-ps laser pulses at high intensities [17].

The objective of this chapter is to determine the applicability of the two-step model and to establish regimes of non-equilibrium radiation heating during intense picosecond laser pulse heating of metal films. The relationships between reflectivity changes and electron and lattice temperatures were first established. Reflectivity changes of gold films during and after 35-ps laser pulse heating were then measured and compared directly with predictions

based on the one-step (Fourier model) and two-step model.

2.2 Experimental System

Temperature measurements during ultrashort light-material interactions are challenging. A lattice-temperature probe with 160-ps resolution was demonstrated based on the reflection high-energy electron diffraction technique [16]. Wang *et al.* measured electron temperature in a highly excited gold target using femtosecond thermionic emission [14]. Surface reflectivity is used in this work as an experimental parameter to indicate electron temperature and lattice temperature during picosecond laser heating.

Figure 2-1 shows a schematic diagram of the experimental system. A YAG laser is used to generate 35-ps laser pulses (full width at half maximum) at 532 nm. The original laser pulse is split into three pulses by beam splitters BS1 and BS2: an intense heating pulse, an reference pulse, and a probe pulse. The intensity of the probe and reference pulses is less than 1% of the heating pulse. As a result, the probe and reference pulses do not produce additional heating effect. The reference pulse is to determine the pulse energy. The delay between the probe and heating pulses can be varied from 0 ps to 1000 ps by changing the optical-path-length of the probe beam. The probe and heating laser pulses are focused onto a 1-μm thick gold film with a spot diameter of 0.43 mm. The film was deposited on a Si wafer by electron beam evaporation in high vacuum.

The intensities of the reflected reference and probe pulses are reduced by neutral density filters (N.D.) and are then detected by two photodetectors (D1 and D2). To minimize
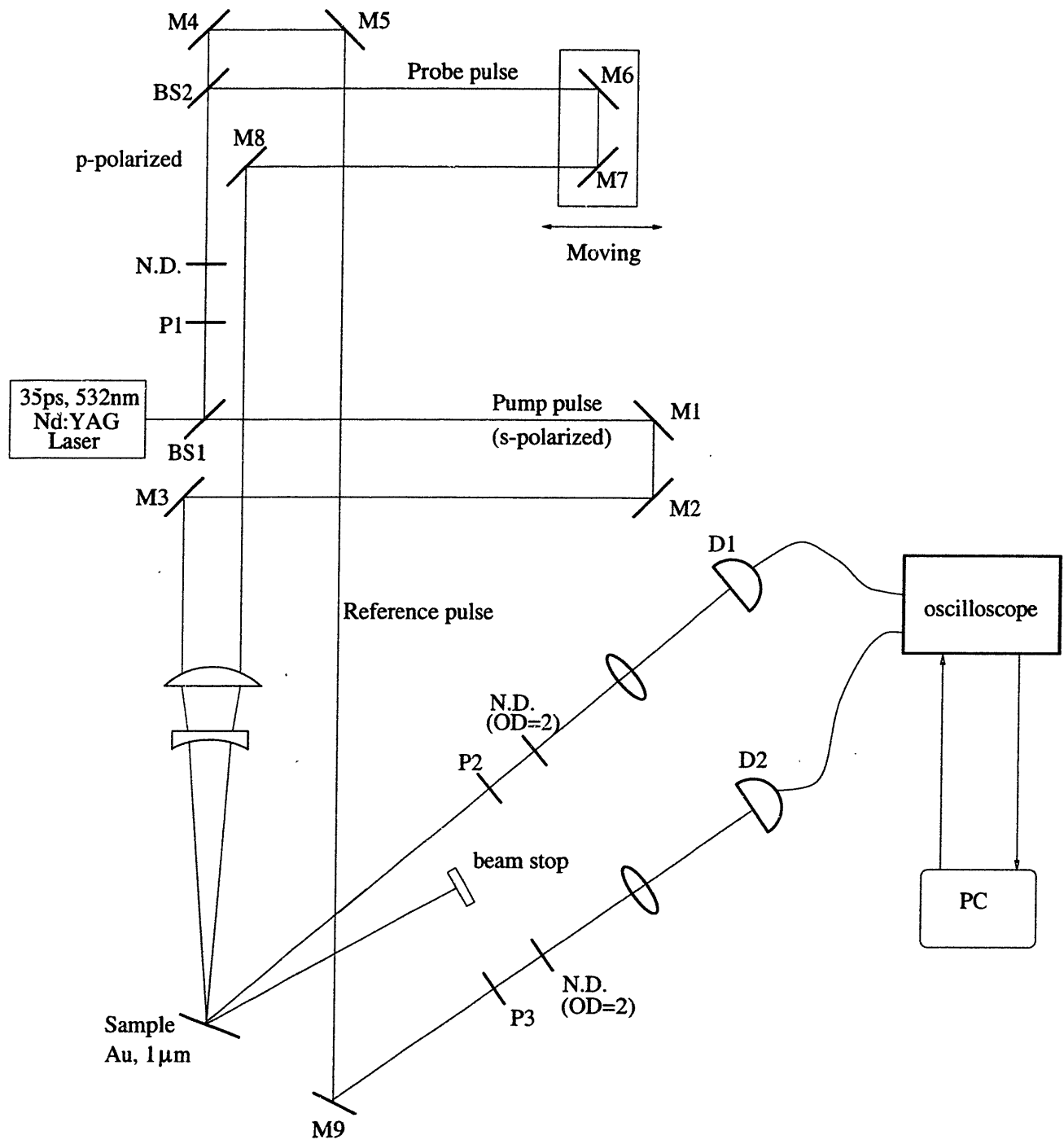
Figure 2-1: Experimental setup.

interference of the intense heating pulse on photodetection, the polarization of the reference and probe pulses are rotated 90 degree relative to the heating beam, and the scattered heating beam is blocked from entering the detectors by two polarizers (P2 and P3). The heating beam is s-polarized, and the probe beam is p-polarized. The angles of incidence of the heating and probe beams are 30° and 26°, respectively.

The photodetectors are calibrated by a power meter. The fluence of the incident heating pulse, J_h, is correlated to the fluence of the reflected reference pulse, J_{ref}, which is measured by detector D2,

$$J_h \;=\; a_1 J_{ref} \tag{2.1}$$

where a_1 is a correlation constant. The fluence of the incident probe beam, J_{p1}, and the fluence of the reflected probe beam when the heating pulse is blocked, J_{p2}, are also correlated to the reflected reference beam,

$$J_{p1} \;=\; a_2 J_{ref} \tag{2.2}$$

$$J_{p2} \;=\; a_3 J_{ref} \tag{2.3}$$

Reflectivity of the film for the probe beam at room temperature, R_0, can be deduced as

$$R_0 \;=\; \frac{J_{p2}}{J_{p1}} = \frac{a_3}{a_2} \tag{2.4}$$

The measured value of R_0 is 0.68. It agrees well with R_0 predicted based on the refractive index of pure gold for p-polarized light at 532 nm at the angle of incidence of 26°

During picosecond laser pulse heating, the surface reflectivity change at a particular delay time can be deduced from the measured fluence of the reflected probe pulse, J_{p3}, which is measured by detector D1,

$$\frac{\Delta R(t)}{R_0} = \frac{R(t) - R_0}{R_0} = \frac{J_{p3} - J_{p2}}{J_{p2}} \tag{2.5}$$

2.3 Energy Transfer Models

Both the one-step and two-step radiation heating models are used to simulate energy transfer processes under the experimental conditions. Since the laser beam diameter (0.43 mm) is much larger than the film thickness, heat conduction parallel to the film surface can be neglected. The electron temperature (T_e) and lattice temperature (T_l) of the film can be described by the one-dimensional, two-step radiation heating model,

$$C_e(T_e)\frac{\partial T_e}{\partial t} = \frac{\partial}{\partial x}\left(k_e\frac{\partial T_e}{\partial x}\right) - G(T_e - T_l) + s(x,t) \tag{2.6}$$

$$C_l(T_l)\frac{\partial T_l}{\partial t} = \frac{\partial}{\partial x}\left(k_l\frac{\partial T_l}{\partial x}\right) + G(T_e - T_l) \tag{2.7}$$

where G characterizes energy exchange between electrons and the lattice, x is the distance measured from the film surface, and C_e and C_l are the electron heat capacity and the lattice heat capacity, respectively. The temporal shape of laser pulses can be approximated as Gaussian. As the maximum reflectivity change during laser pulse heating is less than 7%, the temperature dependence of radiation absorption is neglected here. As a result, the volumetric laser pulse heating term, $s(x,t)$, can be descried as Gaussian and independent

of temperature,

$$s(x,t) = \frac{0.94 J_{abs}}{t_p \delta} \exp\left[-\frac{x}{\delta} - 2.77\left(\frac{t}{t_p}\right)^2\right] \qquad (2.8)$$

where δ is the radiation penetration depth, and J_{abs} is the laser fluence absorbed by the film, $J_{abs} = (1 - R_s)J_h$. For the s-polarized heating beam, the reflectivity of the gold film, R_s, is found to be 0.74 in this work.

Since the thermal diffusion depth in gold within 1 ns is around 0.3 μm, shorter than the film thickness, the effect of silicon substrate on picosecond laser heating of the film is negligible. Both the front and back surfaces of the film can be modelled as insulting boundaries.

For comparison, the conventional one-step radiation model is also simulated,

$$C(T)\frac{\partial T}{\partial t} = \frac{\partial}{\partial x}\left(k\frac{\partial T}{\partial x}\right) + s(x,t) \qquad (2.9)$$

Both the two-step and one-step models are solved numerically with the semi-implicit Crank-Nicholson scheme. Parameters used in simulations are listed in table 2.1. The reported temperature dependent thermal conductivity, $k(T_l)$, and lattice heat capacity, C_l, are used [18,19]. For pure gold, free electrons contribute 99% of total heat conduction [20]. Thermal conductivity of the lattice system is

$$k_l(T_l) = 0.01 k(T_l) \qquad (2.10)$$

Thermal conductivity of free electrons is affected by both the electron temperature and

Table 2.1: Parameters used in simulation.	
Initial temperature (T_0)	300 K
Laser pulse duration (t_p)	35 ps
Film thickness (L)	1 μm
Electron heat capacity at $T_0(C_e(T_e) = \gamma T_e)$	2.1×10^4 Jm^{-3}K^{-1}
Electron-lattice coupling factor G	2.6×10^{16} Wm^{-3}K^{-1}
Radiation penetration depth (δ)	20.6 nm

lattice temperature [14],

$$k_e(T_e, T_l) = 0.99k(T_l)\frac{T_e}{T_l + BT_e^2} \tag{2.11}$$

where $B = 0.0001$ K^{-1}.

Figure 2-2 presents predicted surface temperatures during 35-ps laser pulse heating. The absorbed laser fluence is 10 mJ/cm^2. The two-step model predicts significant non-equilibrium heating during the initial 100 ps. After the initial 200 ps, the surface temperatures of the lattice predicted from the one-step model and two-step model are identical.

2.4 Temperature Dependence of Reflectivity

Reflectivity of metals is a weak function of temperature. From a microscopic point of view, the lattice temperature affects gaps between energy bands, and the electron temperature determines the distribution of electrons. Parkins reported optical properties of gold at 532 nm at 78 K, 22°C and 152°C [21]. Figure 2-3 shows the calculated temperature coefficient of reflectivity,
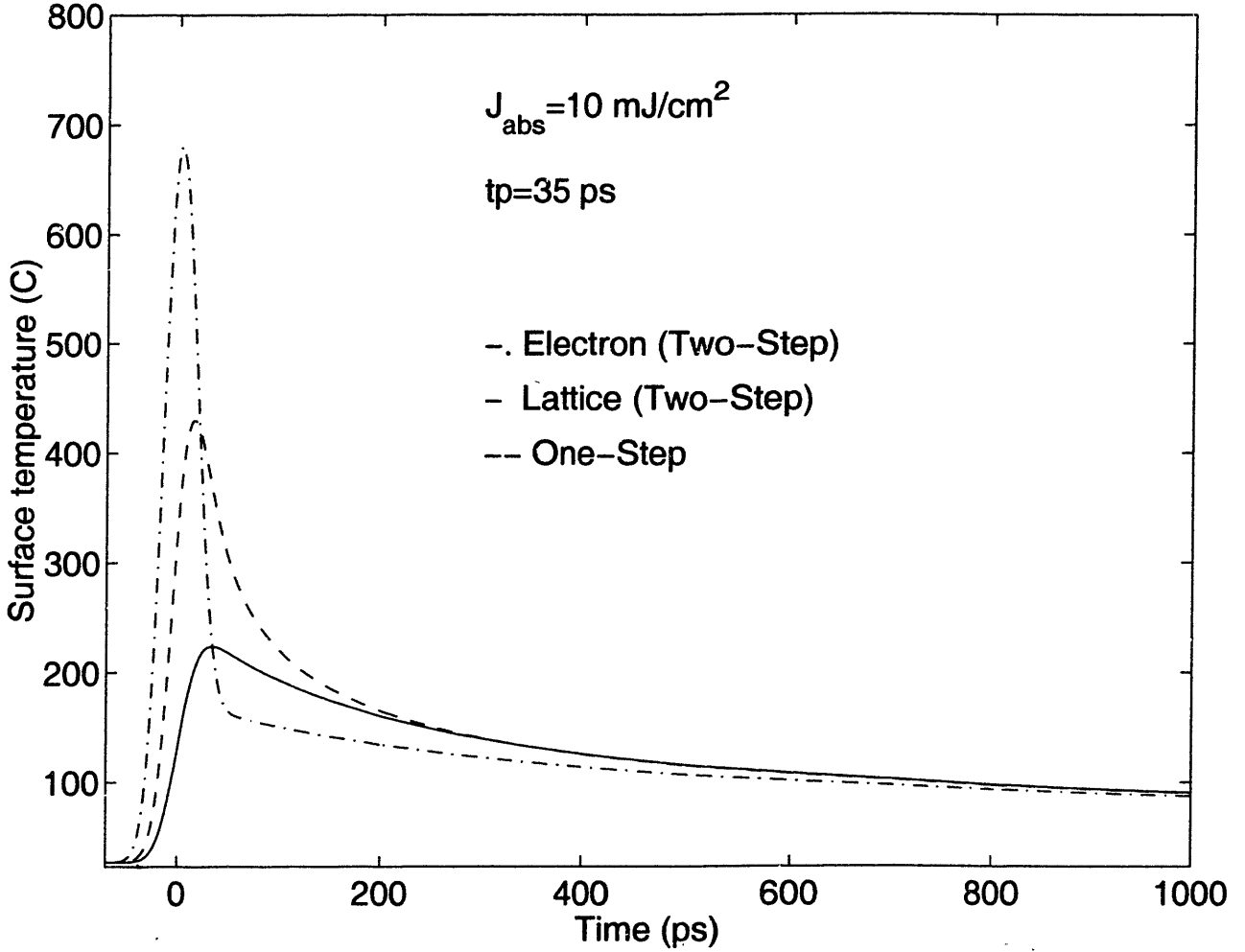
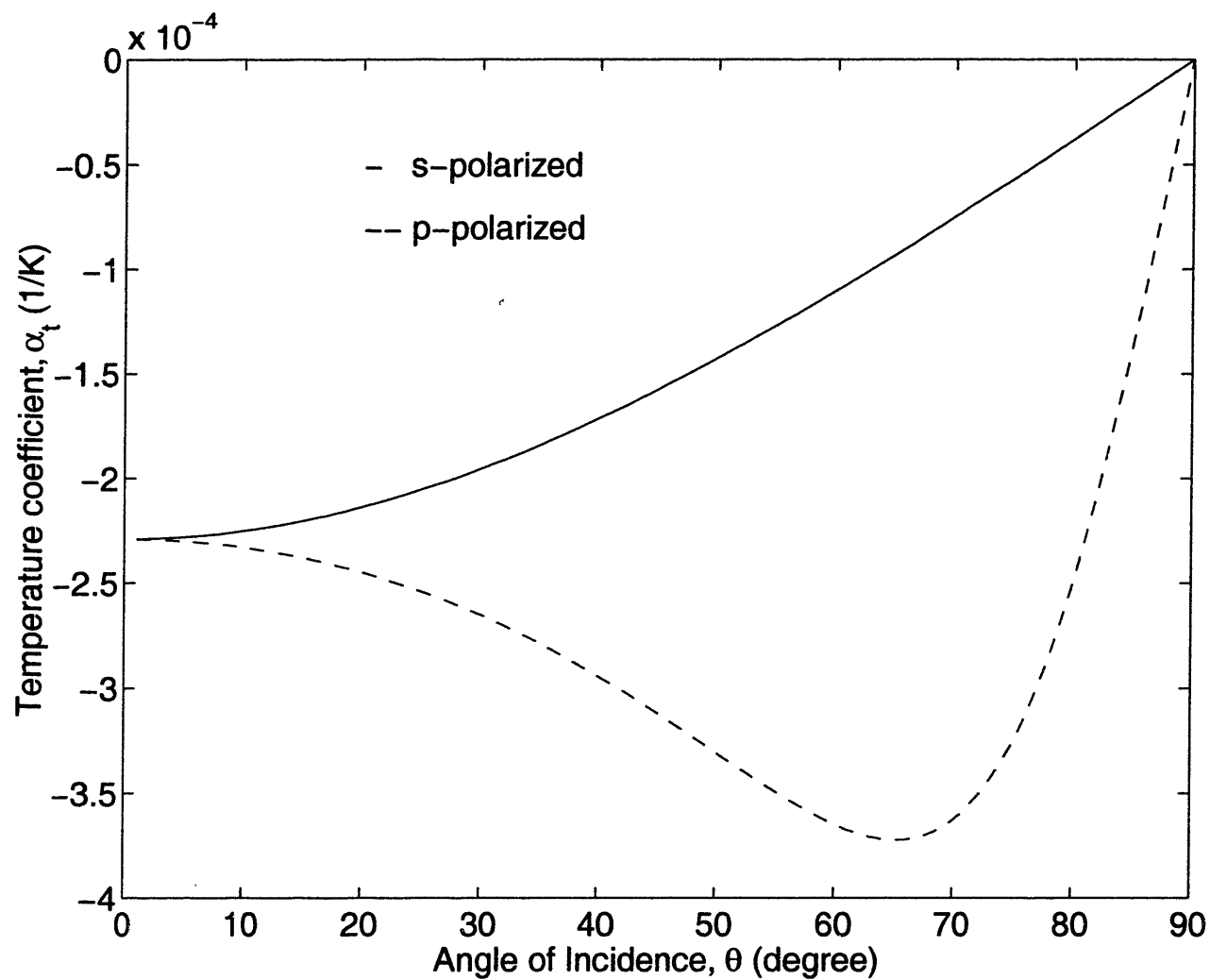Figure 2-2: Predicted transient surface temperature during picosecond laser heating.

Figure 2-3: Averaged temperature coefficient of reflectivity of gold at 532 nm between 22°C and 152°C.

$$\alpha_t \;=\; \frac{1}{R}\frac{dR}{dT} \approx \frac{R(T_1) - R(T_2)}{R(T_1)(T_1 - T_2)} \tag{2.12}$$

based on Parkins' data for s- and p-polarized light beams averaged over the temperature range from 77 K to 152°C.

In this work, the temperature coefficient of reflectivity is deduced experimentally. After the initial 200 ps of laser pulse heating, both the one-step and two-step models predict identical temperatures. The dependence of the surface temperature on laser fluence, $\left(\frac{dT}{dJ_{abs}}\right)_t$, can be predicted accurately. At a fixed time delay, the dependence of reflectivity on laser fluence is measured, $\left(\frac{dR}{RdJ_{abs}}\right)_t$. The temperature coefficient of reflectivity then can be deduced from the slopes of the measured reflectivity curve and predicted temperature curve,

$$\alpha_t \;=\; \frac{1}{R}\frac{dR}{dT} = \frac{dR}{RdJ_{abs}}\frac{dJ_{abs}}{dT} \tag{2.13}$$

The temperature coefficient of reflectivity deduced at different delay times is presented in Table 2.2. These deduced values are consistent with that calculated based on Parkins' data, -2.5×10^{-4} K^{-1}, averaged over the temperature range from 78 K to 152°C for p-polarized light at the angle of incidence of 26°. As expected, the deduced temperature coefficient is independent of the delay time within the experimental error.

Table 2.2: Temperature coefficient of reflectivity of gold at 532 nm.

Delay time (ps)	200	300	400	600	800	1000
Temp. range (K)	300-500	300-510	300-490	300-460	300-440	300-425
$\alpha_t \times 10^4$ (K^{-1})	−2.6	−2.7	−2.7	−2.7	−2.7	−2.2

22

When the electron and lattice systems are not in thermal equilibrium, the surface reflectivity change is affected by both the electron temperature and lattice temperature,

$$\frac{\Delta R}{R_0} = \alpha_t \left[a(T_{e,s} - T_0) + (1 - a)(T_{l,s} - T_0) \right] \tag{2.14}$$

where $T_{e,s}$ and $T_{l,s}$ are the electron temperature and lattice temperature at the film surface, respectively. The percentage contribution of the electron system to the total reflectivity change, a, is found to be 18% by comparing measured reflectivity change at $t_d = 0$ ps with predicted electron and lattice temperatures (Fig. 2-4).

2.5   Picosecond Laser Heating

This section compares model predictions directly with experimental results to evaluate the applicability of the one-step and two-step radiation heating models during picosecond laser heating. The predicted temperatures are used to calculate transient reflectivity.

Figure 2-5 shows the typical temperature profiles near the film surface at 0 ps and 50 ps during 35-ps laser pulse heating. Both the electron temperature and lattice temperature are uniform within the 20-nm radiation penetration depth. As a result, the effect of temperature gradients on reflectivity can be neglected [22], and the transient reflectivity can be determined by the electron and lattice temperatures at the surface.

Due to the finite duration of the probe pulse, the measured reflectivity change is the
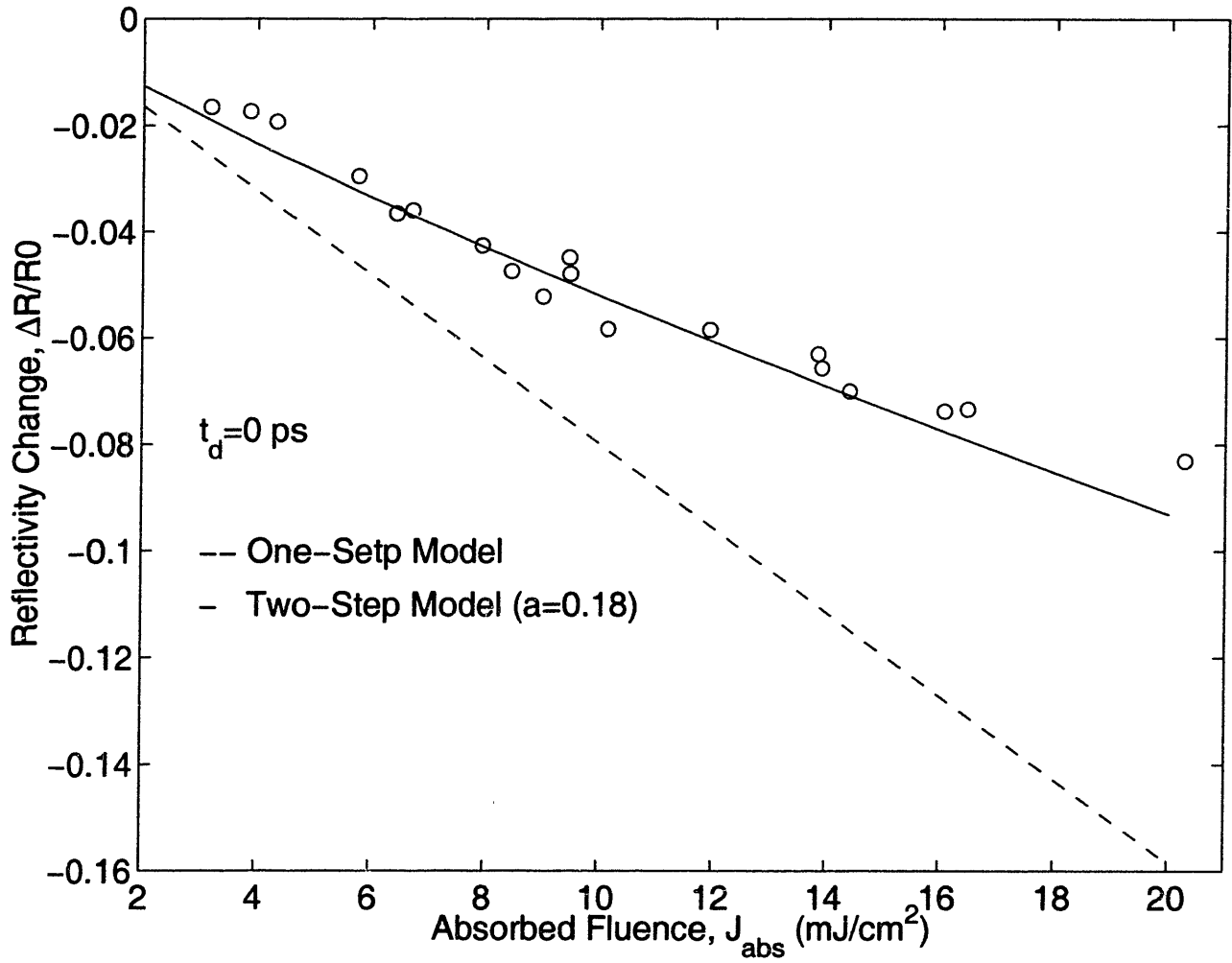
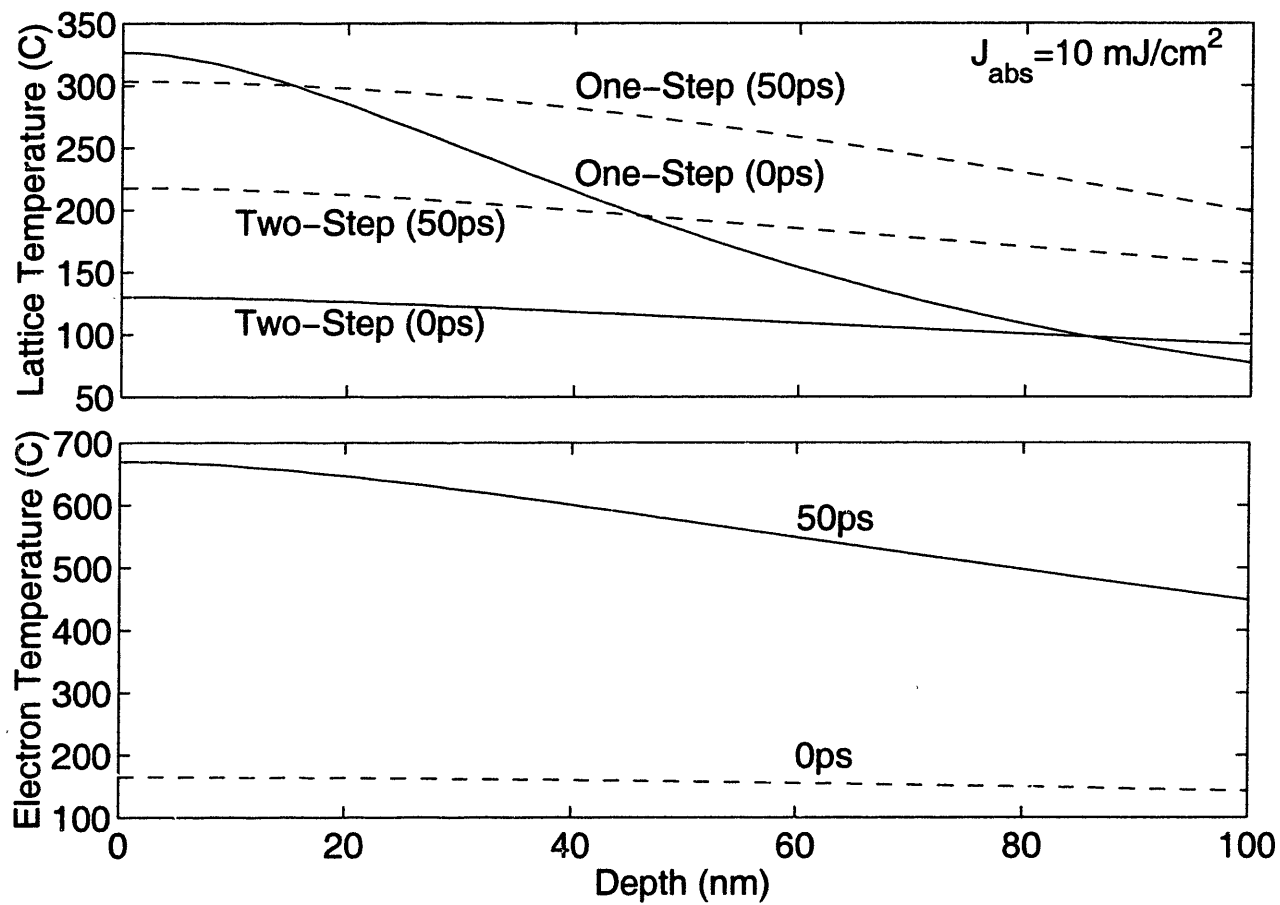Figure 2-4: Contribution of the electron temperature rise to reflectivity change.

Figure 2-5: Predicted temperature profiles.

convolution of transient reflectivity over the duration of the probe laser pulse,

$$\frac{\Delta R(t)}{R_0} \quad = \quad \frac{1.06}{t_p} \int_{-\infty}^{\infty} \alpha_t \left\{ a\left[T_{e,s}(\tau) - T_0\right] + (1 - a)\left[T_{l,s}(\tau) - T_0\right] \right\} \exp\left[-2.77\left(\frac{\tau - t}{t_p}\right)^2\right] d\tau$$

Figure 2-6 compares measured and predicted reflectivity changes during 35-ps laser pulse heating. The absorbed laser fluence is 10 mJ/cm^2. Prediction of the two-step radiation heating model agrees well with the experimental results during the entire time span, from 0 ps to 1000 ps. On the other hand, the one-step, Fourier model over-predicts the reflectivity change by as large as 90% during the initial 100 ps of laser pulse heating. After the initial 200 ps, both models agree well with experimental results. The results show that 35-ps laser pulse heating of gold films involves significant microscopic energy transfer processes. It takes about 200 ps for electrons to reach thermal equilibrium with the lattice. The two-step model predicts a maximum lattice temperature of 220°C which occurs well after the end of the heating laser pulse (Fig. 2-2). By neglecting microscopic energy transfer steps between photons, electrons and the lattice, the Fourier model predicts a maximum lattice temperature of 690°C near the end of the laser pulse. The lattice temperature is over-predicted by 300%.

Figures 2-7 and 2-8 present transient reflectivity changes of the gold film during picosecond laser heating at lower and higher laser fluences. At the absorbed laser fluence of 4 mJ/cm^2 and 20 mJ/cm^2, the maximum lattice temperature rise is around 100°C and 450°C, respectively. The two-step model agrees well with the experimental results within this temperature range.

26
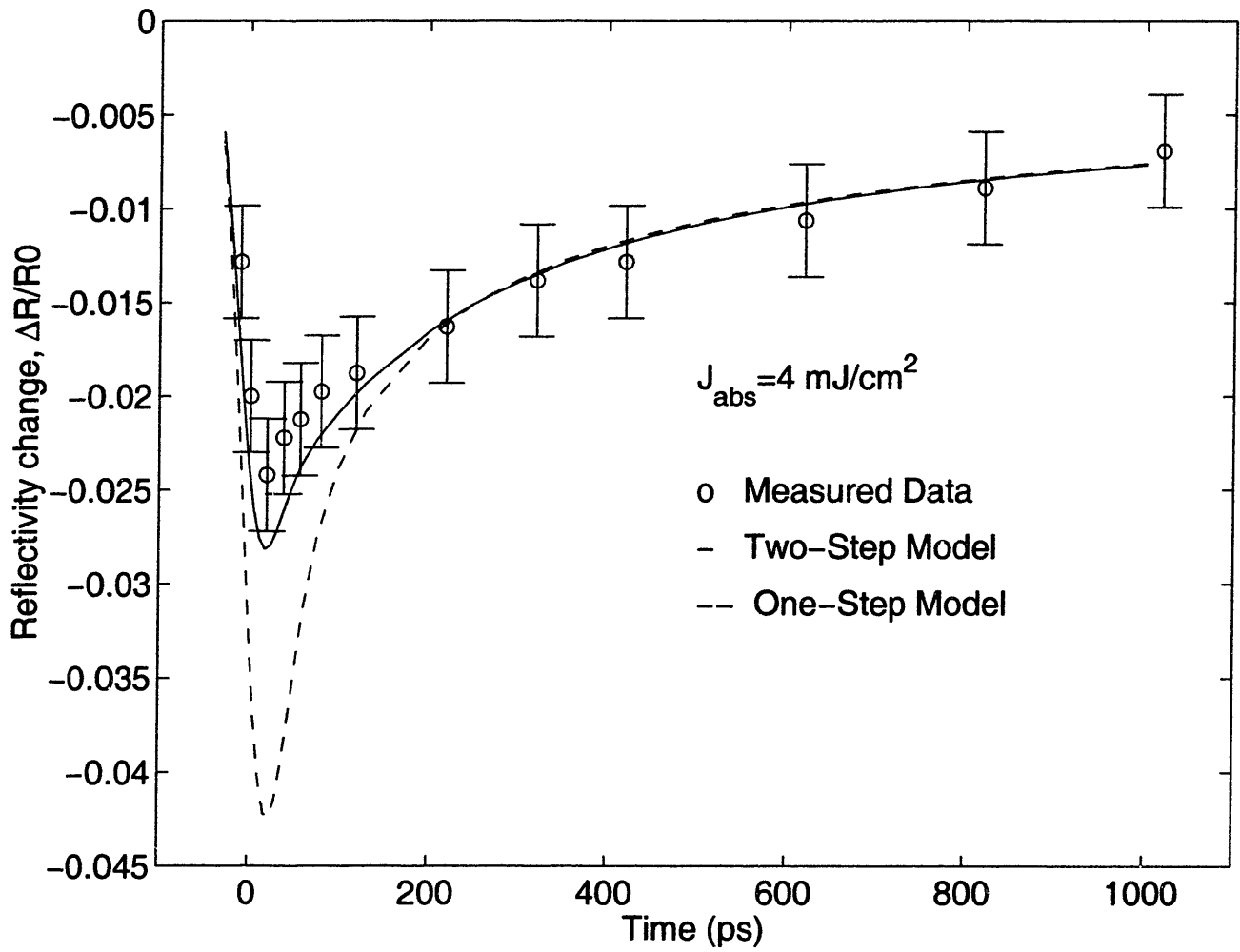
Figure 2-6: Comparison of measured and predicted reflectivity change during picosecond laser heating ($J_{abs} = 4$ mJ/cm^2).
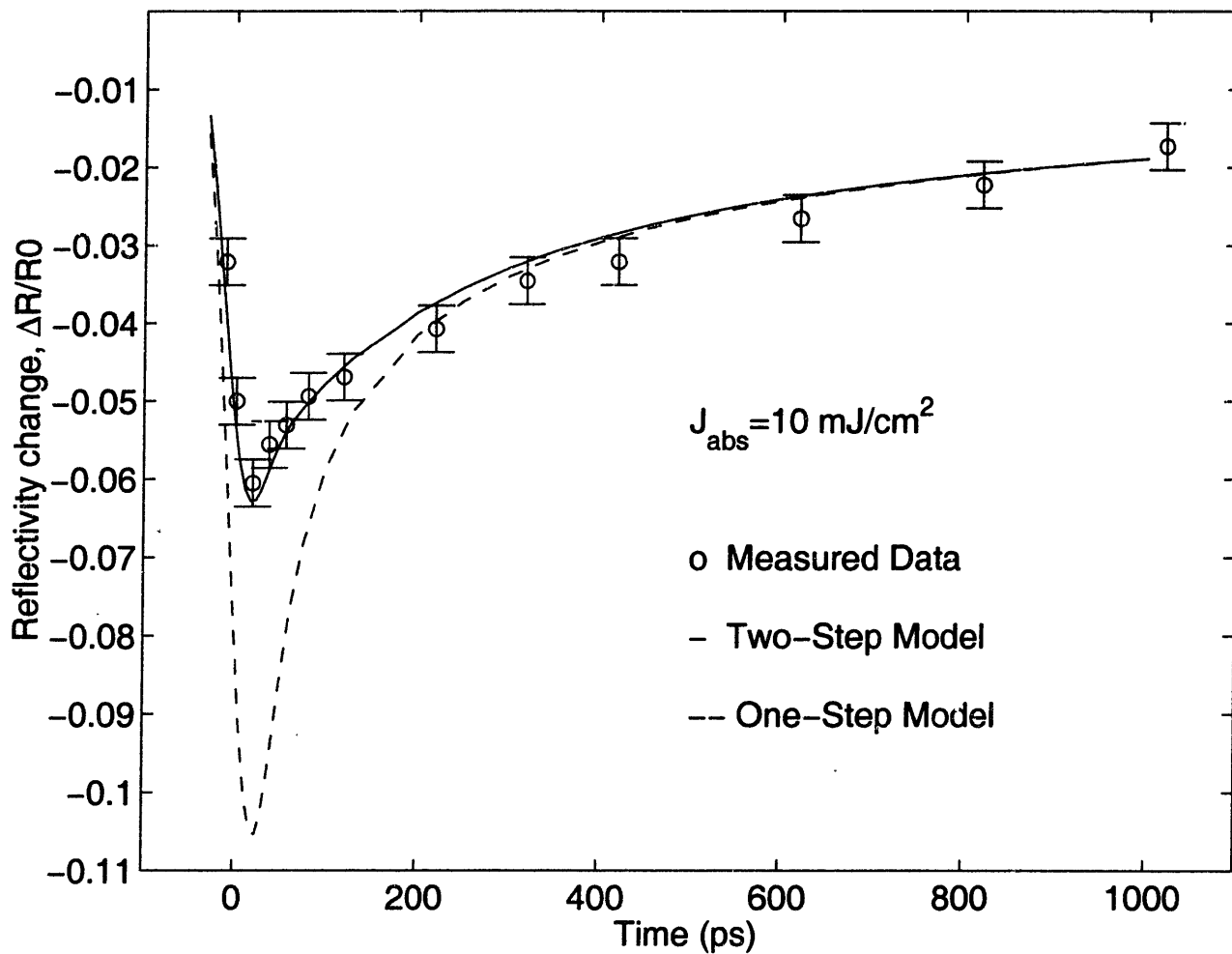
Figure 2-7: Comparison of measured and predicted reflectivity change during picosecond laser heating ($J_{abs} = 10$ mJ/cm^2).
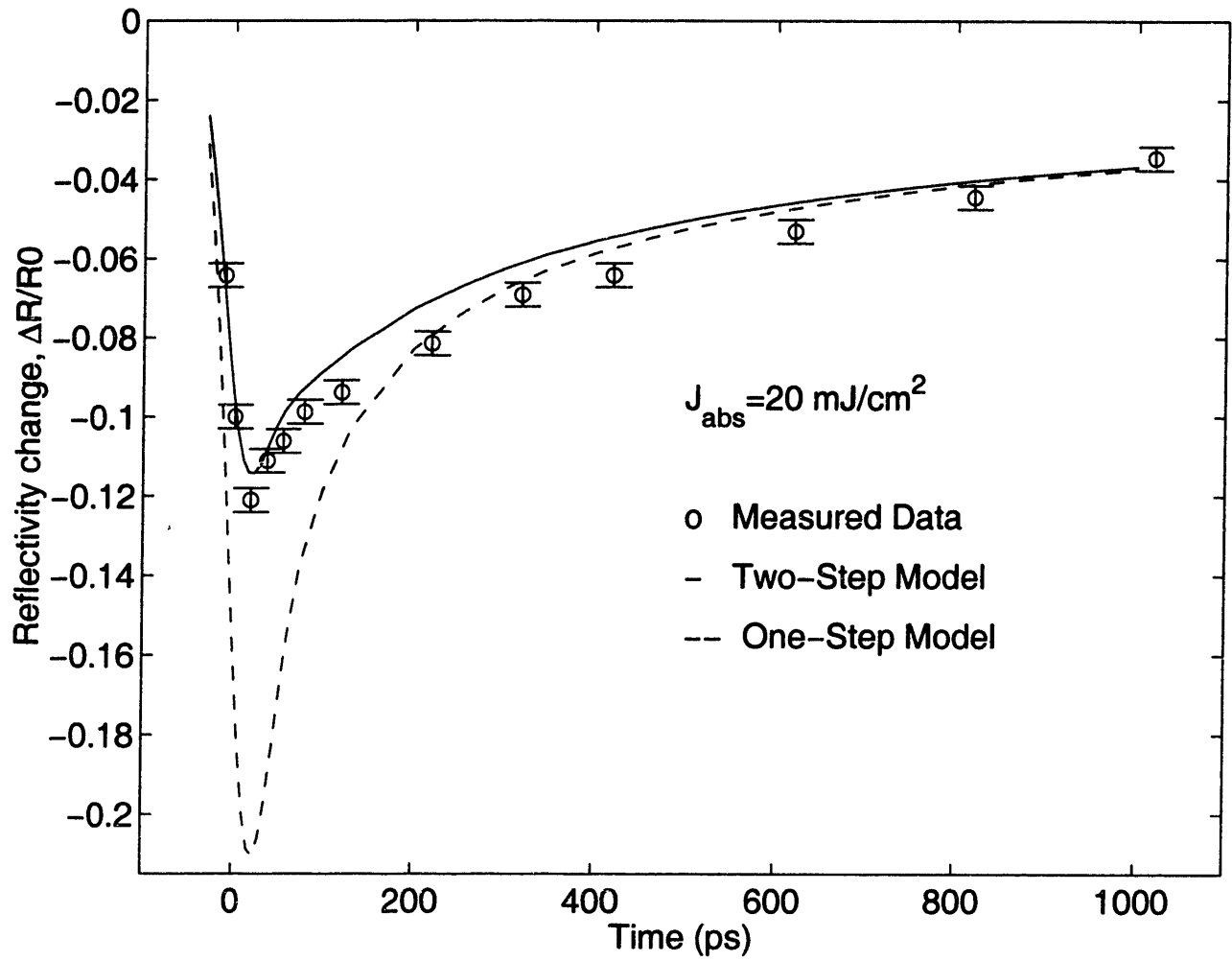
Figure 2-8: Comparison of measured and predicted reflectivity change during picosecond laser heating (J_{abs} = 20 mJ/cm^2).

2.6 Conclusions

Picosecond experiments have been conducted to investigate energy transfer mechanisms during intense laser pulse heating of metal films. Measured reflectivity changes are compared with model predictions. Results show that microscopic energy-transfer processes between photons, electrons and the lattice have significant effect during picosecond laser-metal interactions. The two-step radiation heating model of metals is found accurate during intense as well as weak laser pulse heating over the entire picosecond regime.

Chapter 3

Non-equilibrium Phase Change

3.1 Introduction

Short-pulse lasers have been applied widely in material processing due to their excellent capability to precisely control the size of the heat-affected region, heating rate, and solidification speed. Examples include laser surface-hardening, laser annealing, and laser micro-machining. Phase change is a crucial phenomenon in short-pulse laser processing of materials. For laser microfabrication, it is important to accurately control the size of the melting region to avoid thermal damage to surrounding devices. In laser annealing and laser hardening applications, it is necessary to accurately control the solidification speed to achieve the desired microstructures of materials. During long-pulse laser processing, melting and solidification processes can be described by conventional thermal models [24,40]. For ultrashort-laser-pulse processing of materials, the applicability of these macroscopic models is subject to question [6].

Laser melting of metal films involves three important microscopic processes: (1) absorp-

tion of photon energy by free electrons, (2) energy transfer between electrons and the lattice [6,7], and (3) initiation of phase change of the lattice. In applications of ultrashort laser pulses, these microscopic processes become important. For example, when the laser-pulse duration is comparable with or less than the electron-lattice thermalization time, which is typically of the order of picoseconds for metals, electrons and the lattice are not in thermal equilibrium during the laser-heating process. Such non-equilibrium energy-deposition has been found significant during picosecond and femtosecond (10^{-15}s) laser heating [8,12,15]. On the other hand, rapid phase-change phenomena are often controlled by nucleation dynamics instead by heat transfer at the liquid-solid interface. During rapid melting, the interface can be heated well above the melting temperature (superheating); while during rapid solidification, the interface can be cooled far below the melting point (undercooling). These non-equilibrium phase-change phenomena have also been observed during picosecond laser melting processes [26,38]. Effects of non-equilibrium energy deposition on phase change, however, have not been studied.

This chapter is to develop a general model to characterize both the non-equilibrium electron-lattice heating process and the non-equilibrium phase-change process for ultrashort-laser-pulse processing of metal films. Picosecond laser melting of gold films is simulated to illustrate the importance of microscale energy transfer.

3.2 Non-equilibrium Energy Deposition and Non-equilibrium Phase Change Model

Deposition of photon energy and initiation of phase change are the two fundamental processes in laser melting. From a microscopic point of view, laser energy is first absorbed by free electrons and then transferred to the lattice through electron-lattice collisions. A two-step radiation heating model has been described in the previous chapter (Eq. 2.6 and 2.7).

At sufficiently high laser power, the melting process can be initiated. During a slow phase-change process, the interface velocity is heat-flow controlled,

$$L_v \vec{u} = -(k\nabla T)^l + (k\nabla T)^s \tag{3.1}$$

where superscript s and l represent the solid phase and the liquid phase, respectively, L_v is the latent heat of fusion per unit volume, and $\vec{u}$ is the interface velocity. During a rapid phase-change process, however, the interface velocity is controlled by nucleation dynamics (Cerny et al., 1991), which can be characterized by the transition state theory (Jackson and Chalmers, 1956; Turnbull, 1962). In this work, the modified transition state theory proposed by Tsao et al. (1986) is used to describe the interface velocity,

$$u = u_s f \exp\left(-\frac{Q}{k_b T_{l,int}}\right) \left[\exp\left(-\frac{\Delta S}{k_b}\right) - \exp\left(-\frac{L_m}{k_b T_{l,int}}\right)\right] \tag{3.2}$$

where u_s is the maximum interface velocity, f is the fraction of sites at the interface where rearrangement of atoms can occur, Q is the activation enthalpy per atom, ΔS is entropy

difference per atom between the liquid state and the solid state, L_m is the latent heat of fusion per atom, k_b is the Boltzmann constant, and $T_{l,int}$ is the lattice temperature at the interface. At a liquid-solid interface, there exists a continuous interchange of atoms between the two phases. Atoms in the liquid phase release the latent heat and rearrange themselves to form crystals. The rate of this solidification process is governed by the entropy difference between the ordered solid state and the disordered liquid state, $\exp(-\Delta S/k_b)$. On the other hand, atoms in the solid phase absorb energy and become disordered. This melting process is controlled by the enthalpy barrier between the liquid and solid phases, $\exp(-L_m/k_b T_{l,int})$. The net rate of atoms solidified or melted is, therefore, proportional to $\exp(-\Delta S/k_b) - \exp(-L_m/k_b T_{l,int})$.

For most metals, the fraction, f, is near unity [30], and the interface velocity is limited by collisions of atoms at the interface [34]. The maximum interface velocity, u_s, is approximately the speed of sound in the liquid phase [23,32]. Homan *et al.* [28] measured melting velocities in gold films and found that the activated enthalpy, Q, is zero for gold. Using the relation of $\Delta S = L_m/T_m$, where T_m is the melting temperature, equation (3.2) can be rearranged as

$$u \;=\; V_0 \left[1 - \exp\left(-\frac{L_m}{k_b T_m} \cdot \frac{T_m - T_{l,int}}{T_{l,int}} \right) \right] \tag{3.3}$$

where V_0 equals to $u_s \exp(-L_m/k_b T_m)$.

3.3 Numerical Simulations

Picosecond laser melting of free-standing gold films is simulated in this work to illustrate the importance of non-equilibrium energy-deposition on ultrashort-laser-pulse processing (Fig. 3-1). During picosecond laser melting, the heat penetration depth in metals is much smaller than laser-beam diameters. Laser melting of metal films, therefore, can be described as a one-dimensional process.

The initial conditions for electrons and the lattice used for simulation are

$$T_e(x, -2t_p) \quad = \quad T_l(x, -2t_p) = T_0 \tag{3.4}$$

During picosecond laser melting, heat losses form film surfaces can be neglected, resulting in thermal-insulation conditions.

$$\frac{\partial T_e}{\partial x}(0, t) \quad = \quad \frac{\partial T_e}{\partial x}(L, t) = \frac{\partial T_l}{\partial x}(0, t) = \frac{\partial T_l}{\partial x}(L, t) = 0 \tag{3.5}$$

The temporal shape of a laser pulse is assumed as Gaussian and the absorbed photon energy is then described by Eq. (2.8) The current two-step model consists of two coupled energy equations (Eq. 2.6 and 2.7) and a nonlinear interface-velocity equation (Eq. 3.3), and the conventional one-step model consists of an energy equation (Eq. 2.9) and the interface-velocity equation (Eq. 3.3). Both models are solved numerically in this work.

During laser melting, the local thermal state of materials, e.g., energy and phase, cannot be uniquely determined by temperature. An enthalpy variable is thus necessary to char-
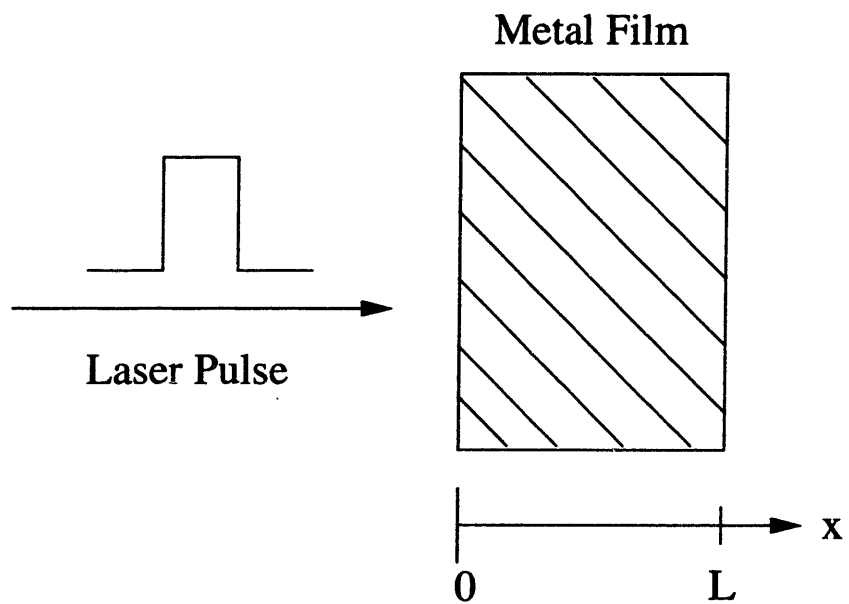
Figure 3-1: Schematic diagram of picosecond laser melting of a metal film

acterize energy of the lattice system [27,33]. By introducing the enthalpy as a variable, equation (2.9) in a one-dimensional form becomes

$$\frac{\partial H}{\partial t} = \frac{\partial}{\partial x}(k\frac{\partial T}{\partial x}) + S \tag{3.6}$$

and equation (2.7) can be re-written as

$$\frac{\partial H_l}{\partial t} = \frac{\partial}{\partial x}(k_l\frac{\partial T_l}{\partial x}) + G(T_e - T_l) \tag{3.7}$$

These energy equations are then transformed into finite difference equations by integration over each control volume (Fig. 3-2) and over a small time interval. The electron and lattice temperatures and material properties are assumed uniform in each control volume. The heat flux, q_{i-1} , crossing the interface between two control volumes, $i - 1$ and i, is determined by the temperature difference, $T_{i-1} - T_i$, and an effective thermal conductivity, $k_{eff,i-1}$. The effective thermal conductivity, $k_{eff,i-1}$, is evaluated from the conductivity of the two control volumes, k_{i-1} and k_i, as

$$k_{eff,i-1} = \frac{2k_i k_{i-1}}{k_i + k_{i-1}} \tag{3.8}$$

If a control volume contains both solid and liquid, its thermal conductivity of this control volume is determined as

$$\frac{k^s k^l}{r k^l + (1-r)k^s} \tag{3.9}$$
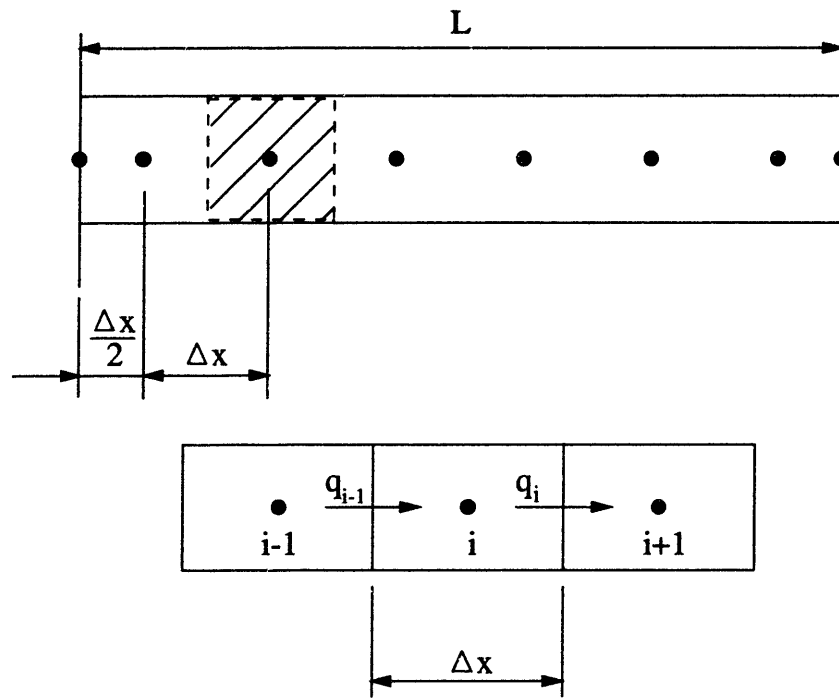
where r is the fraction of solid in the control volume.

Figure 3-2: Schematic diagram of control volumes

Table 3.1: Time steps and number of grid points used in simulation

	20 ps		1 ps	
	one-step	two-step	one-step	two-step
time step (ps)	0.005	0.05	0.005	0.05
grid number	800	2500	800	2500

The forward Euler method is used first to estimate the interface velocity, u, solid fraction, r_i, and enthalpy H_i, in each control volume. The lattice temperature, $T_{l,i}$, is then determined from the enthalpy-temperature relation,

$$H_i(T_{l,i}) = r_i H^s(T_{l,i}) + (1 - r_i) H^l(T_{l,i}) \qquad (3.10)$$

The enthalpy-temperature relation, $H^s(T_l)$ and $H^l(T_l)$ used in this work is calculated from the heat capacity data and is shown in Figure 3-3. Second, the electron temperature is solved from the energy equation of electrons by semi-implicit scheme. The temperatures at the present time step and the previous time step are then used to determine the averaged material properties, interface velocity, and heat flux between these two time steps. The solution steps are repeated with the updated values until both the electron and lattice temperatures reach convergence requirements $(\Delta T_e / T_{e,0} \leq 10^{-4}, \Delta T_l / T_{l,0} \leq 10^{-5})$. The corresponding time steps and the number of grid points used in simulation are given in Table 3.1. The total increase of energy in the electron and lattice systems is compared with absorbed radiation energy,

$$\int_0^L \int_{-2t_p}^t S(x, t) dt dx \qquad (3.11)$$

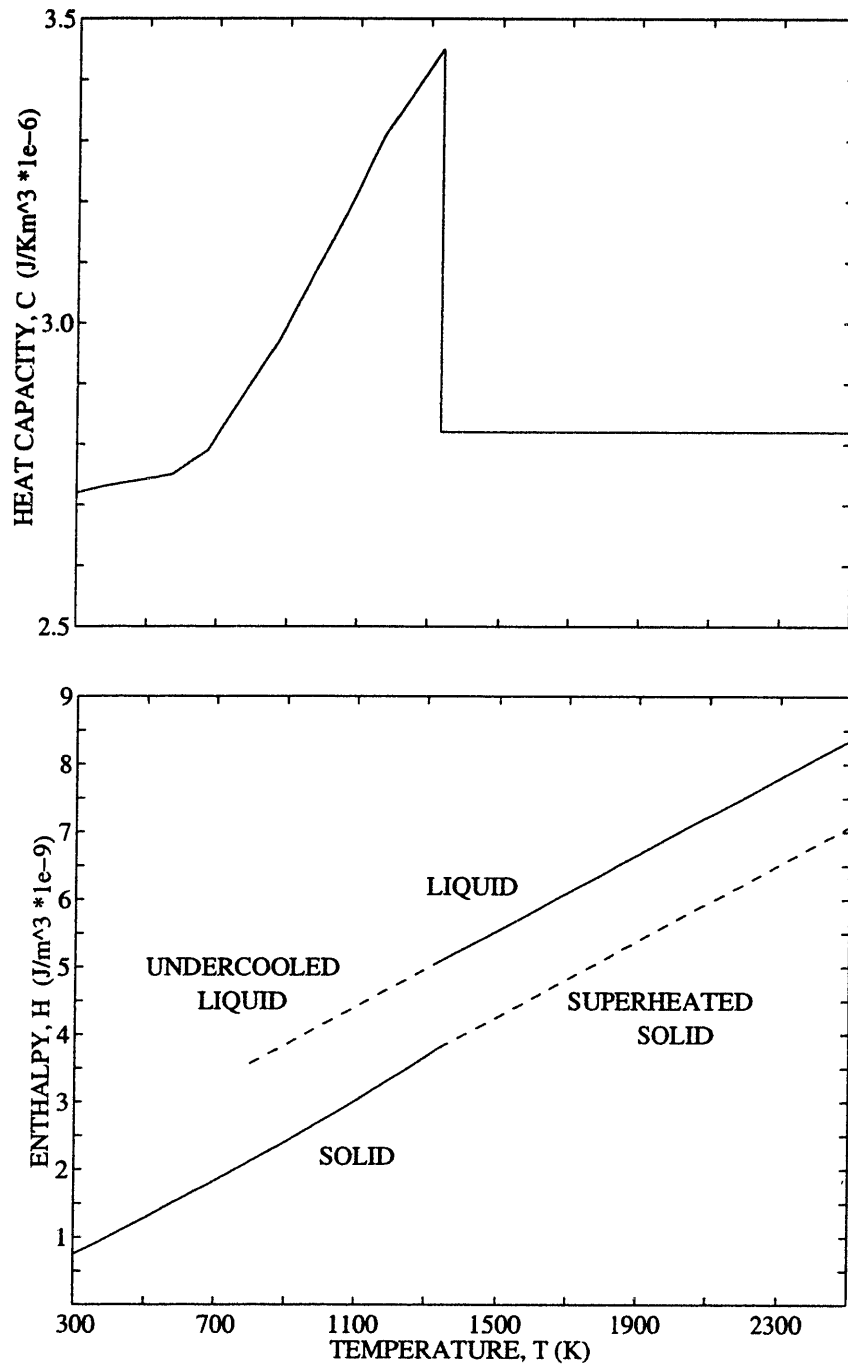The difference is within 0.1% in this work.

Figure 3-3: Temperature-dependent heat capacity and enthalpy

Table 3.2: Physical properties of gold used in simulation

Initial temperature (T_0)	300 K
Electron heat capacity at $T_0(C_{e,0})$	2.1×10^4 Jm^{-3}K^{-1}
Electron-lattice coupling factor G	$^s2.6 \times 10^{16}$ Wm^{-3}K^{-1}
	$^l3.1 \times 10^{16}$ Wm^{-3}K^{-1}
Reflectivity (R)	0.6
Radiation penetration depth (δ)	20.6 nm
Melting point (T_m)	1336 K
Limit velocity (V_0)	1300 ms^{-1}

s: Solid state; l: Liquid state

Table 3.3: Thermal conductivity of gold [18]

Solid Phase[a]		Liquid Phase[a]	
Temperature	Thermal conductivity	Temperature	Thermal conductivity
(K)	(Wm^{-1}K^{-1})	(K)	(Wm^{-1}K^{-1})
300	315	1336	105
500	309	1400	106
600	304	1500	109
800	292	1600	112
1100	271	1800	116
1200	262	2000	120
1300	251	2400	124
1336	247	2600	125

The physical properties of gold used in this simulation are given in Table 3.2, Table 3.3, and Figure 3-3. Note that the electron heat capacity is proportional to the electron temperature [31]. In metals, both free electrons and the lattice contribute to heat conduction. The conventionally measured thermal conductivity, k, is the sum of the electron thermal conductivity, k_e, and the lattice thermal conductivity, k_l. In gold, k_e is ninety-nine percent of k, and k_l is only one percent of k [20]. Since atoms in the liquid phase do not have long-range orders, electrons collide more frequently with liquid atoms as compared to periodically arranged atoms in solid crystals. The electron-lattice coupling factor of molten gold is assumed, therefore, to be 20% above the value of solid gold in this work. Because

of the lack of thermal properties of superheated or undercooled gold, material properties at the melting point are used for these non-equilibrium states.

3.4   Results and Discussion

Figure 3-4 shows the predicted surface temperature of a 1 μm gold film during 20-ps laser melting based on both the current two-step model and the conventional one-step model. In the one-step model, absorbed photon energy is converted directly to lattice energy, and the surface temperature follows the temporal shape of the laser pulse. On the other hand, The two-step model predicts a delayed response of the lattice temperature since photon energy is absorbed first by electrons and then transferred to the lattice gradually through electron-lattice collisions.

During picosecond laser heating, non-equilibrium electrons carry absorbed photon energy far away from the radiation-absorption region before these electrons transfer absorbed photon energy to the lattice. This non-equilibrium energy-deposition process leads to a much larger heat-affected region and a much smaller temperature rise of the lattice.

For the one-step model, there is a kink in the graph corresponding to 130 ps time delay. This point indicates the end of the solidification process since the thermal conductivity in the solid state phase is different from that in the liquid phase.

Figure 3-5 presents the transient melting depth, interface temperature, and interface velocity during 20-ps laser melting of a 1 μm gold film. The one-step model and the two-step model predict significantly different results. First, based on the conventional one-step
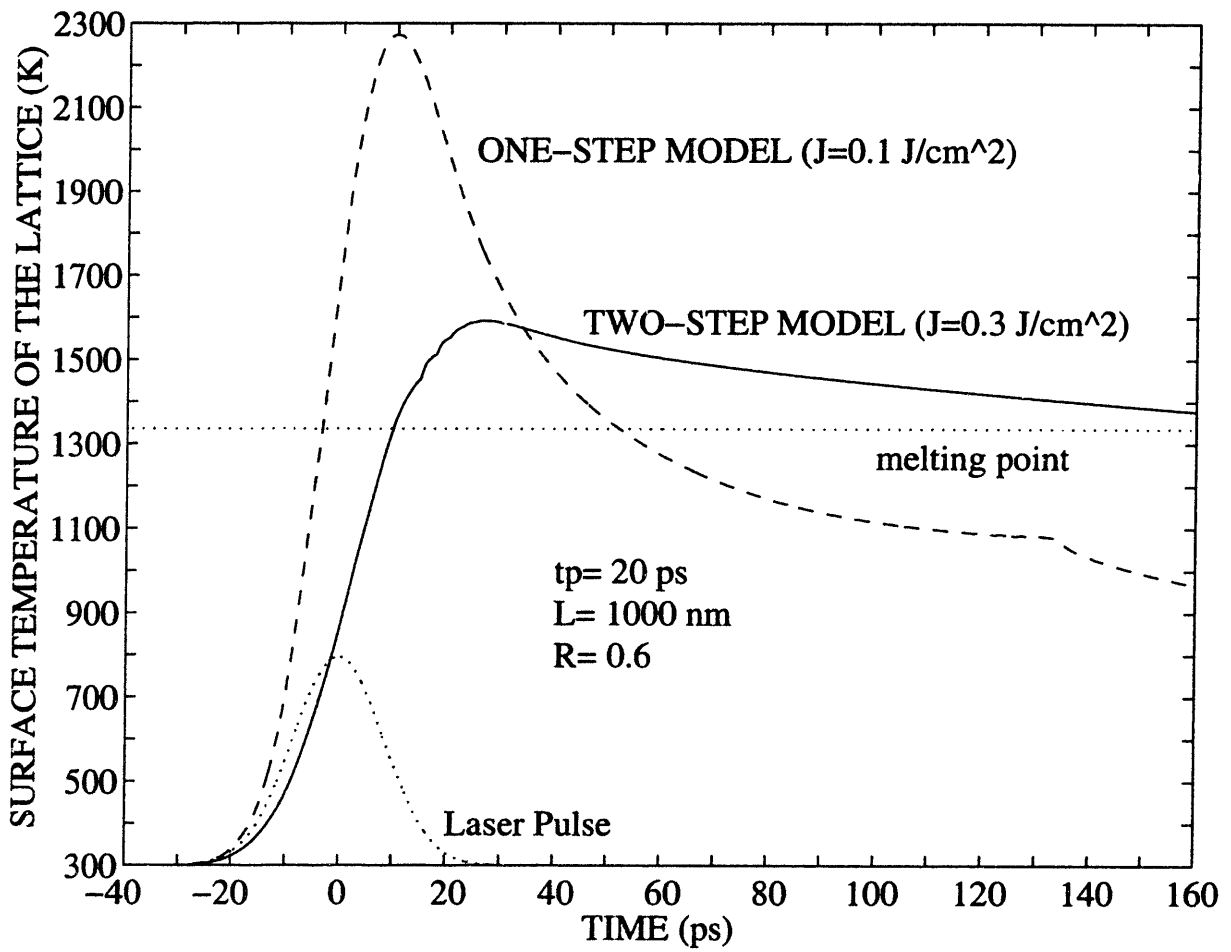
Figure 3-4: Predicted surface temperature during 20-ps laser melting of a 1 μm gold film
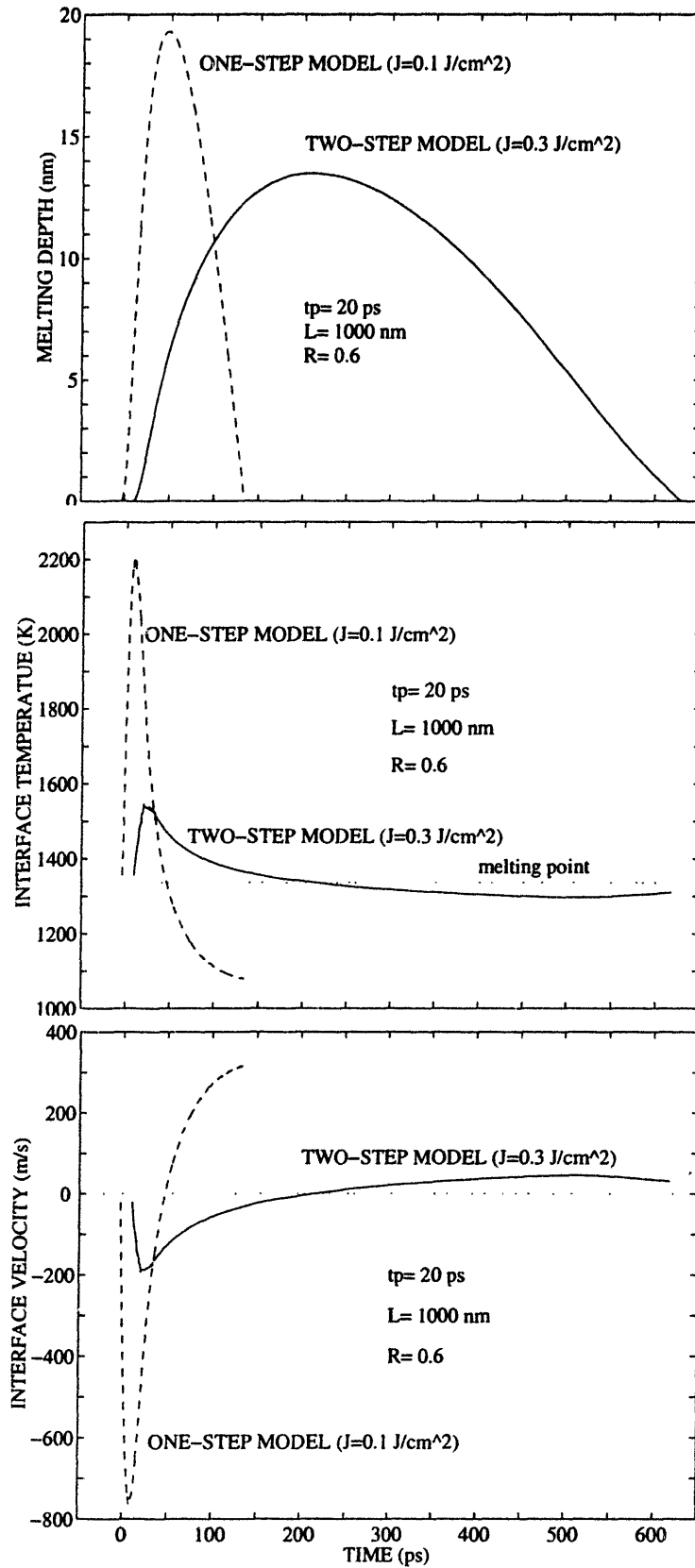
Figure 3-5: Transient phase change during 20-ps laser melting

model, the film surface always starts melting during laser pulse irradiation; while based on the current two-step model, the melting process is initiated near or after the end of laser irradiation. This two-step model prediction is consistent with the observed picosecond delay of the initiation of melting during 20-ps laser melting of free-standing aluminum films [39]. Second, the latter model predicts a melting duration about four times longer than that from the former model, which could explain that the measured melting duration is several times longer than that predicted from the conventional one-step model [32]. Third, the two-step model predicts significantly smaller superheating and undercooling, about 200 K and 30 K, respectively, compared to those predicted from the one-step model, around 750 K and 250 K, respectively. Consequently, the maximum melting velocity and solidification speed based on the two-step model are 200 m/s and 50 m/s, respectively, much smaller than those predicted from the one-step model (770 m/s and 320 m/s).

Figure 3-6 shows the temperature profiles in a gold film during 20 ps laser melting. In one-step model predictions, since laser energy is converted to lattice energy directly, the maximum temperature occurs always at the film surface. On the other hand, The two-step model predicts the existence of a maximum lattice temperature within the film. During the melting process, the solid material beneath the liquid-solid interface can be superheated by photo-excited electrons well above the interface temperature. During the rapid solidification process, release of the latent heat of fusion raises the interface temperature above temperatures of the surrounding solid and undercooled liquid.

Although the superheating of the solid can be as high as several hundred degree, the period of time that the solid stays at the superheating state is only about 200 ps. Therefore,
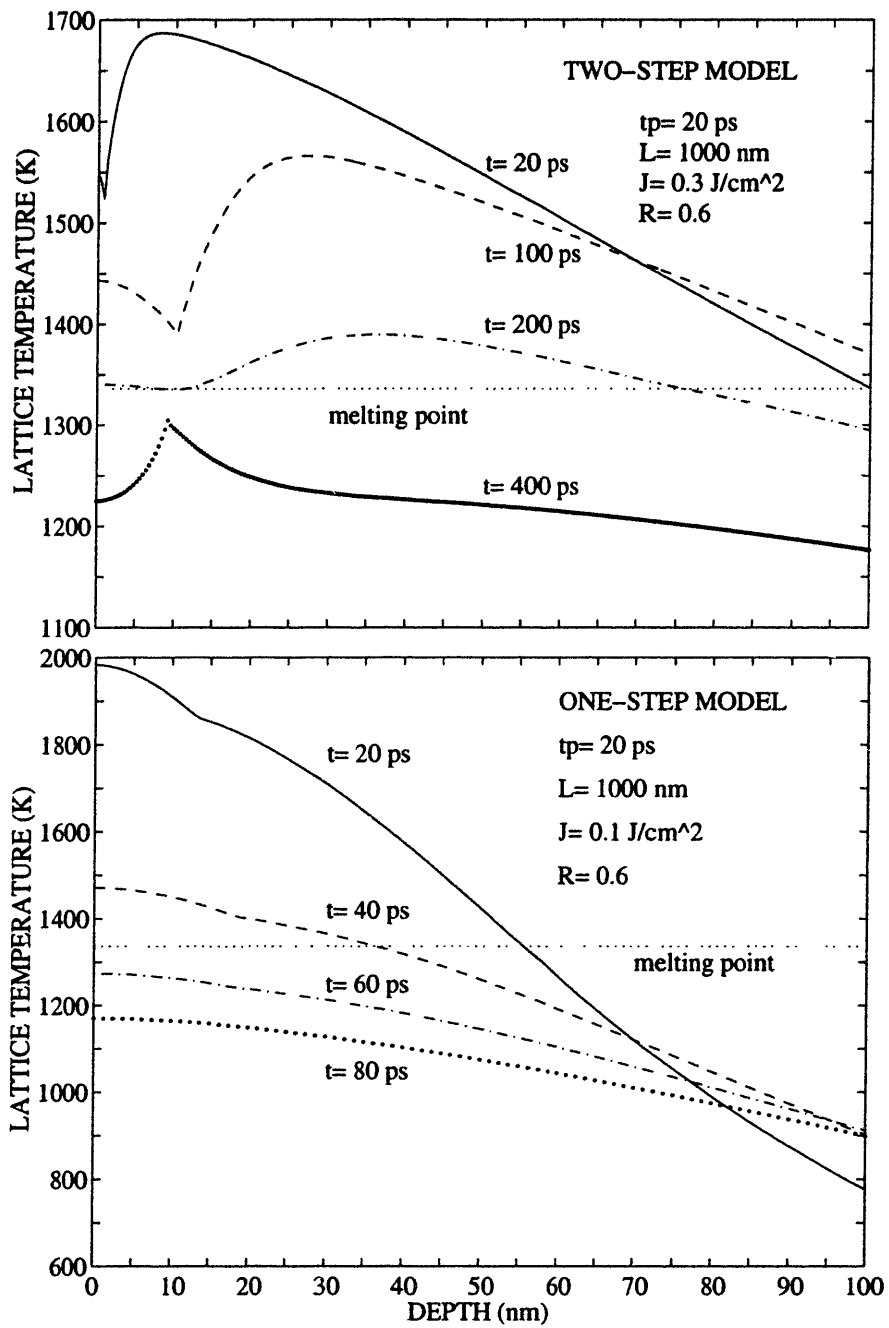
Figure 3-6: Transient temperature profiles in a 1 μm gold film during 20-ps laser melting

the possibility of volumetric phase change is very low and phase change occurs mainly at the interface.

Figure 3-7 presents the predicted surface temperature of a gold film during 1-ps laser melting. The thermal penetration depth based on the one-step model can be approximated as the sum of the radiation penetration and the thermal diffusion length, $\delta + \sqrt{\alpha t_p}$, which decreases with the decrease of laser-pulse duration. As a result, a higher temperature rise is produced during 1-ps laser melting compared to 20-ps laser melting even at a lower energy level (Fig. 3-4). The two-step model, however, predicts a distinctively different dependence of surface temperature rise on laser pulse duration. A shorter laser pulse produces a stronger non-equilibrium heating process and a greater effective thermal conductivity of electrons (Eq. 2.11), which in turn gives rise to a larger thermal-affected region and a smaller lattice temperature rise.

Figures 3-8 and 3-9 show transient phase change during 1-ps laser melting of a 1 μm gold film. By reducing the laser pulse duration by a factor of 20 from 20 ps to 1 ps, the melting depth is reduced to 3.8 nm and 3.2 nm based on the one-step model and the two-step model, respectively. These melting regions are composed of only about ten layers of gold atoms, indicating that picosecond laser pulses can be used to process materials with atomic scale precision.

In continuous-wave and long-pulse laser applications, e.g., the surface hardening and wear-resistance coating, a high solidification speed is often required to form a thin layer of surface material of novel microstructures. The laser-material interaction time is often
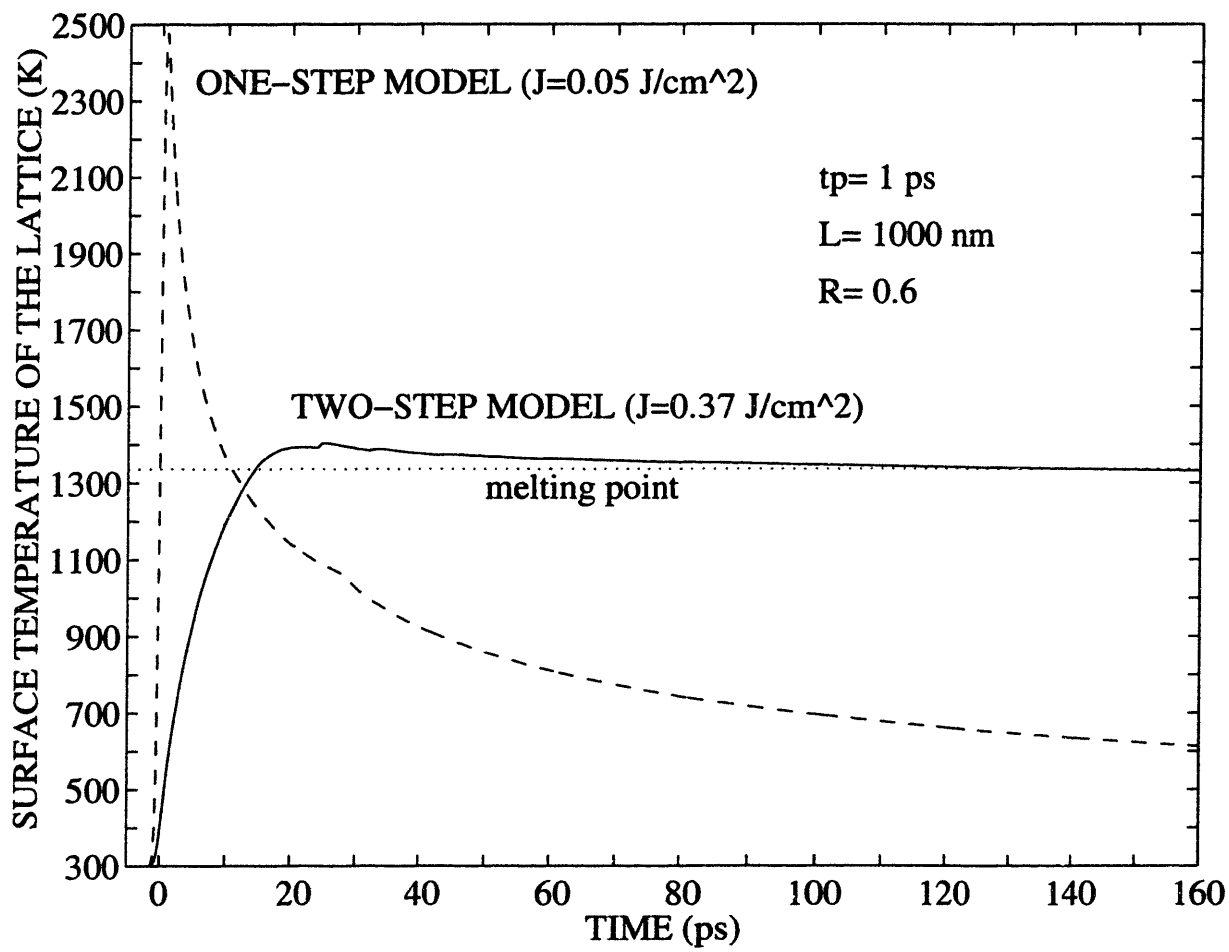
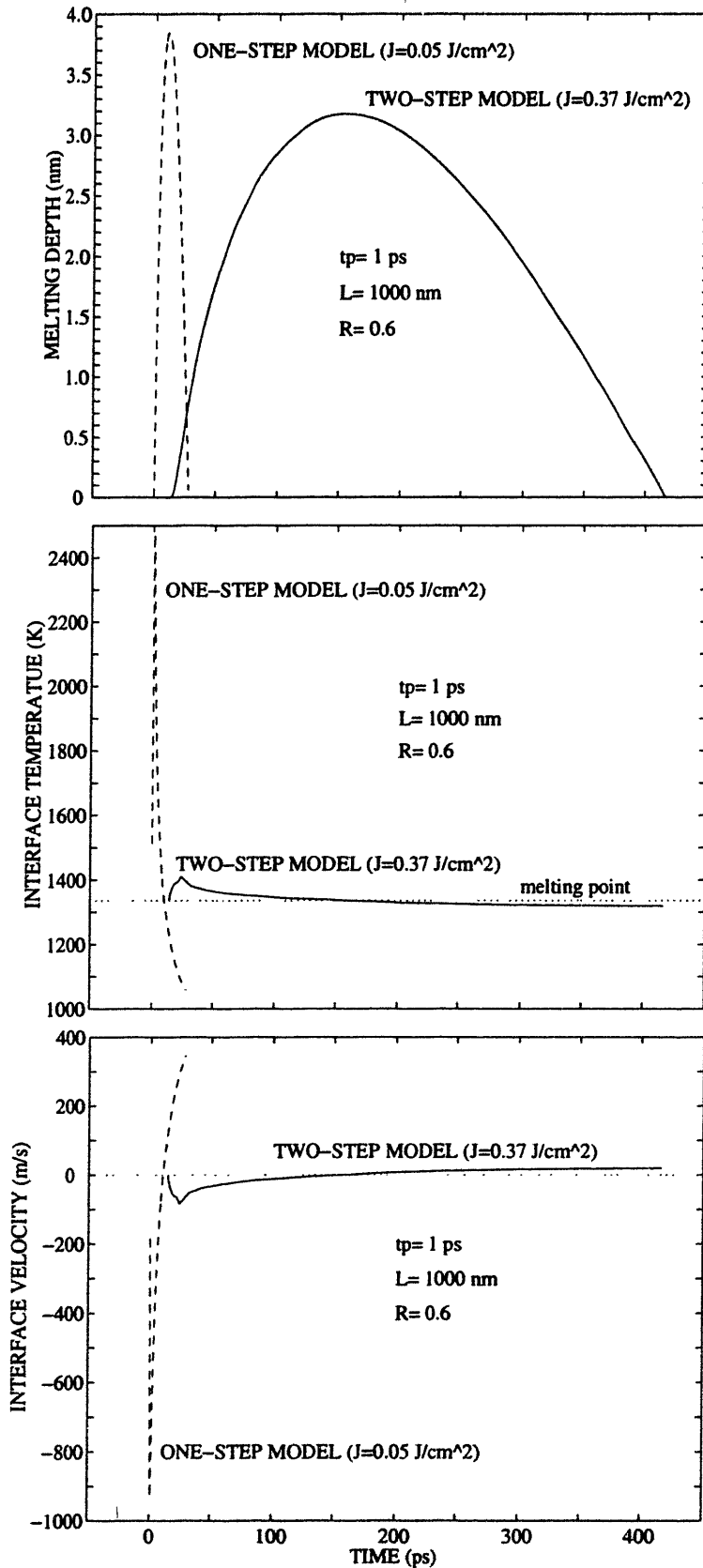Figure 3-7: Surface-temperature response during 1-ps laser melting

Figure 3-8: Transient melting depth, interface temperature and velocity during 1-ps laser melting
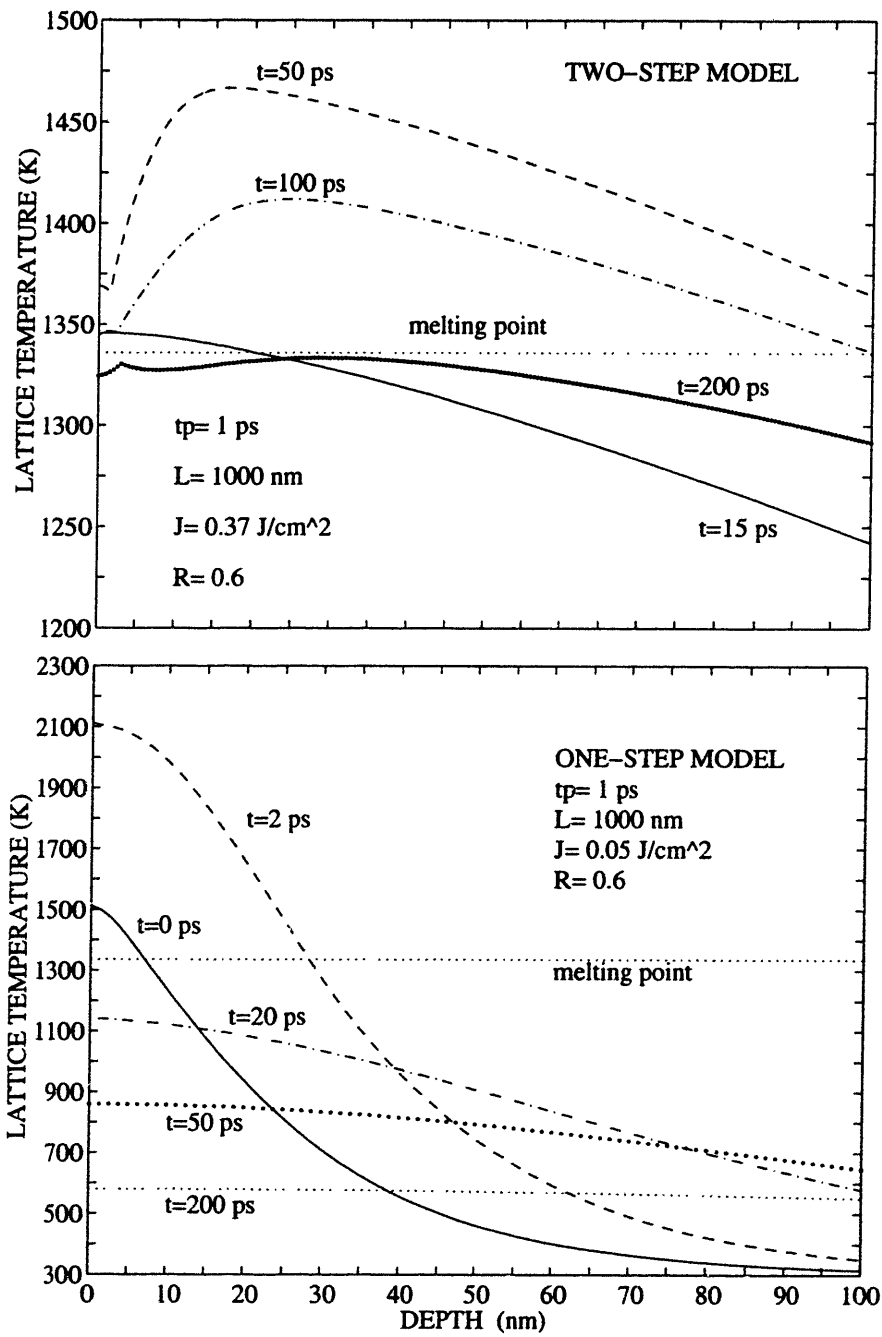
Figure 3-9: Transient temperature profiles during 1-ps laser melting of a 1 μm gold film

reduced in order to increase the solidification speed. The current two-step model, however, shows that for picosecond laser applications, both the melting speed and solidification speed cannot be increased by using laser pulses of a shorter duration. Instead, by reducing the pulse duration from 20 ps to 1 ps, the solidification speed is reduced from 50 m/s to 15 m/s.

The temperature profiles in the gold film during 1-ps laser melting show a significant non-equilibrium energy-deposition process (Fig. 3-9). At time t=15 ps, which is well after laser pulse irradiation, a significant amount of absorbed laser energy is still stored in the electron system. It takes about 50 ps for electrons and the lattice to reach thermal equilibrium.

3.5 Conclusions

In this chapter, a general two-step laser melting model for applications of ultrashort laser pulses was developed. The non-equilibrium energy-deposition process is described by the coupled electron system and the lattice system, and the non-equilibrium phase-change process is characterized by a modified transition state theory. During picosecond laser melting of a gold film, electrons and the lattice are not found in thermal equilibrium. The high mobility of non-equilibrium electrons gives rise to a much larger thermal-affected zone and smaller lattice temperature rise, which in turn significantly reduces the interface velocity and prolongs the melting duration. These results indicate that microscopic energy transfer and phase change are significant for picosecond laser processing of materials.

Chapter 4

Conclusions and Future Work

4.1 Conclusions of Current Work

In chapter 2, picosecond experiments have been conducted to observe energy transfer processes during intense laser pulse heating of metal films. Measured reflectivity changes indicate that microscopic energy transfer mechanisms have significant impacts during picosecond laser-metal interactions. The two-step radiation heating model for metals is demonstrated to be accurate during intense ultrashort laser pulse heating. This is the first work, according to the author's knowledge, to compare quantitatively the experimental results with model predictions.

In chapter 3, a general non-equilibrium energy deposition and non-equilibrium phase change model was developed. During picosecond laser melting of a metal film, the high mobility of non-equilibrium electrons lead to a much larger thermally affected region and lower lattice temperature rise, which in turn increases the melting threshold, reduces the interface velocity, and prolongs the phase change processes.

4.2 Future Work

An theoretical model is needed to describe optical properties of material during non-equilibrium laser heating. Temperature dependence of optical properties has been widely studies. These works, however, were based on thermal equilibrium conditions and are not accurate when the materials are not in thermal equilibrium. It is not clear the relative contributions of electrons and the lattice on the temperature effect. For example, the electron temperature in metals affects the optical properties by affecting electron distributions. On the other hand, the lattice temperature affects the lattice spacing and the vibrations of the ions themselves, which results in distortions of the energy band.

Future research is needed to investigate experimentally the validity of the non-equilibrium phase change theory. Based on the current experimental setup, a longer time delay is necessary to observe the complete phase change processes.

Laser interactions with semiconductors and insulators are an important topic, not only for fundamental research but also for industry applications. How to characterize energy transfer and phase change during ultrashort pulse laser irradiation is an inevitable question to develop more reliable and accurate picosecond and femtosecond technologies.

REFERENCES

[1] Lin, H. N., Stoner, R. J., Maris, H. J., 1990, " Nondestructive Testing of Microstructures by Picosecond Ultrasonics," *J. Nondestructive Evaluation*, Vol. **9**, pp. 239-246.

[2] Eesley, G. L., 1990, "Picosecond Dynamics of Thermal and Acoustic Transport in Metal Films," *Int. J. of Thermophysics*, Vol. **11**, pp. 811-815.

[3] Solis, J., Siegel, J., Garcia, C., and Jimenez, J., 1997, "Nanocrystalline Ge Synthesis by Picosecond Pulsed Laser Induced Melting and Rapid Solidification," In: *Advances in microcrystalline and nanocrystalline semiconductors*, Materials Research Society, Boston (Massachusetts, USA), Collins RW, editor, pp. 839-44.

[4] Sonnleitner, M., Schutz, G. J., and Schmidt, T., 1990, "Imaging Individual Molecules by Two-Photon Excitation," *Chemical Physics Letters*, Vol. **300**, pp. 221-226.

[5] Piston, D. W., 1999, "Imaging Living Cells and Tissues by Two-Photon Excitation Microscopy," *Trends in cell biology*, Vol. **9**, pp. 66-69.

[6] Anisimov, S. I., Kapeliovich, B. L., and Perel'man, T. L., 1974, "Electron Emission from Metal Surfaces Exposed to Ultrashort Laser Pulses," *Sov. Phys. JETP*, Vol. **39**, pp. 375-377.

[7] Qiu, T. Q., and Tien, C. L., 1993, "Heat Transfer Mechanisms during Short-Pulse Laser Heating of Metals," *Journal of Heat Transfer*, Vol. **115**, pp. 835-841.

[8] Eesley, G. L., 1983, "Observation of Nonequilibrium Electron Heating in Copper," *Phys. Rev. Lett.*, Vol. **51**, pp. 2140-2143.

[9] Eesley, G.L., 1986, "Generation of Nonequilibrium Electron and Lattice Temperatures in Copper by Picosecond Laser Pulses," *Phys. Rev. B* Vol. **33**, pp. 2144-2151.

[10] Schoenlein, R. W., Lin, W.Z., and Fujimoto, J.G., 1987, "Femtosecond Studies of Nonequilibrium Electronic Processes in Metals," *Phys. Rev. Lett.*, Vol. **58**, pp. 1680-1683.

[11] Elsayed-Ali, H. E., Norris, T. B., Pessot, M. A., and Mourou, G.A., 1987, "Time-Resolved Observation of Electron-Phonon Relaxation in Copper," *Phys. Rev. Lett.*, Vol. **12**, pp. 1212-1215.

[12] Brorson, S. D., Fujimoto, J. G., and Ippen, E. P., 1987, "Femtosecond Electronic Heat-Transfer Dynamics in Thin Gold Films," *Phys. Rev. Lett.*, Vol. **59**, pp. 1962-1965.

[13] Fann, W. S., Storz, R., Tom, H. W. K., and Boker, J., 1992, "Direct Measurement of Nonequilibrium Electron-Energy Distributions in Subpicosecond Laser-Heated Gold Films," *Phys. Rev. Lett.*, Vol. **68**, 2834-2837.

[14] Wang, X. Y., Riffe, D.M., Lee, Y-S, and Downer, M.C., 1994, "Time-Resolved Electron-Temperature Measurement in a Highly Excited Gold Target Using Femtosecond Thermionic Emission," *Phys. Rev. B*, Vol. **50**, pp. 8016-8019.

[15] Qiu, T. Q., Juhasz, T., Suarez, C., Bron, W. E., and Tien, C.L., 1994, "Femtosecond Laser Heating of Multi-layer Metals-II. Experiments," *Int. J. Heat Mass Transfer*, Vol. **37**, pp. 2799-2808.

[16] Elsayed-Ali, H. E., and Herman, J. W., 1990, "Picosecond Time-Resolved Surface-Lattice Temperature Probe," *Appl. Phys. Lett.*, Vol. **57**, pp. 1508-1510.

[17] Rosenfel, A., and Campbell, E. E. B., 1996, "Picosecond UV-Laser Ablation of Au and Ni Films," *Appl. Surface Science*, Vol. **96-98**, pp. 439-442.

[18] Youloukian, Y. S., Powell, R. W., Ho, C. Y., and Klemens, P. G., 1970, *Thermal conductivity*, IFI/Plenum, New York.

[19] Youloukian, Y. S., and Buyco, E. H., 1970, *Specific heat*, IFI/Plenum, New York.

[20] Klemens, P. G., and Williams, R. K., 1986, "Thermal Conductivity of Metals and Alloys," *Int. Metals Review*, Vol. **31**, pp. 197-215.

[21] Parkins, G.R., 1979, *Temperature Dependence of the Optical Constants of the Noble Metals*, PhD thesis, Dartmouth College, NH.

[22] Lorincz, A., 1990, "Picosecond Transient Thermoreflectance: a Mew Probe of Two-Dimensional and Quasi-Two-Dimensional Structures," *J. Appl. Phys.*, Vol. **67**, pp. 2567-2570.

[23] Aziz, M. J., 1982, "Model for Solute Redistribution during Rapid Solidification," *J. Appl. Phys.*, Vol. **53**, pp. 1158-1168.

[24] Baeri, P., Campisano, S. U., Foti, G., and Rimini, E., 1979, "A Melting Model for Pulsing-Laser Annealing of Implanted Semiconductors," *J. Appl. Phys.*, Vol. **50**, pp. 788-797.

[25] Cerny, R., Sasik, R., Lukes, I., and Chab, V., 1991, "Excimer-Laser-Induced Melting and Solidification of Monocrystalline Si: Equilibrium and Non-equilibrium Model," *Phys. Rev. B*, Vol. **44**, pp. 4097-4102.

[26] Elsayed-Ali, H. E., Herman, J. W., and Murphy, E. A., 1993, "Ultrafast Laser Super-heating of Metal Surfaces," *Mat. Res. Soc. Symp. Proc.*, Vol. **279**, pp. 685-690.

[27] Grigoropoulos, C. P., Dutcher, W. E., Jr., and Emery, A. F., 1991, "Experimental and Computational Analysis of Laser Melting of Thin Silicon Films," *Journal of Heat Transfer*, Vol. **113**, pp. 21-29.

[28] Homan, B. E., Connery, M. T., Harrison, D. E., and MacDonald, C. A., 1993, "Measurements of Melting Velocities in Gold Films on a Picosecond Time Scale," *Mat. Res. Soc., Symp. Proc.*, Vol. **279**, pp. 717-722.

[29] Jackson, K. A., and Chalmers, B., 1956, "Kinetics of Solidification," *Can. J. Phys.*, Vol. **34**, pp. 473-490.

[30] Jackson, K. A., 1958, *Liquid Metals and Solidification*, ASM, Cleveland, Ohio, pp. 174.

[31] Kittel, C., 1986, *Introduction to Solid State Physics*, 6th Edn, Wiley, New York.

[32] MacDonald, C. A., Malvezzi, A. M., and Spaepen, F., 1989, "Picosecond Time-Resolved Measurements of Crystallization in Noble Metals," *J. Appl. Phys.*, Vol. **65**, pp. 129-136.

[33] Miaoulis, I. N., and Mikic, B. B., 1986, "Heat Source Power Requirements for High-Quality Recrystallization of Thin Silicon Films for Electronic Devices," *J. Appl. Phys.*, Vol. **59**, pp. 1658-1662.

[34] Spaepen, F., and Turnbull D., "Formation of Metallic Glasses," in *Rapidly Quenched Metals*, 2nd International Conf., edited by Grant, N. J. and Giessen, B. C.(MIT Press, Cambridge, Massachusetts, 1976), pp. 205-229.

[35] Touloukian, Y. S., and Buyco, E. H., 1970, *Thermophysical Properties of Matter*, Vol.4, Ifi/Plenum, New York-Washington.

[36] Tsao, J. Y., Aziz, M., Thompson, M. O., and Peercy, P., 1986, "Asymmetric Melting and Freezing Kinetics in Silicon," *Phys. Rev. Lett.*, Vol. **56**, pp. 2712-2715.

[37] Turnbull, D., 1962, "On the Relation between Crystallization Rate and Liquid Structure," *J. Phys. Chem.*, Vol.**66**, pp. 609-613.

[38] Von der Linde, D., Fabricius, N., Danielzik, B., and Bonkhofer, T., 1987, "Solid Phase Superheating during Picosecond Laser Melting," *Mat. Res. Symp. Proc.*, Vol. 74, pp. 103-108.

[39] Williamson, S., Mourou, G., and Li, J. C. M., 1984, "Time-Resolved Laser-Induced Phase Transformation in Aluminum," *Phys. Rev. Lett.*, Vol. **52**, pp. 2364-2367.

[40] Wood, R. F., and Giles, G. E., 1981,"Macroscopic Theory of Pulsed-Laser Annealing. I. Thermal Transport and Melting," *Phys. Rev. B*, Vol. **23**, pp. 2923-2942.